

Novel Quartz Clock with Integrated Wireless Energy Harvesting and Sensing Functions

Chaoyun Song, *Member, IEEE*, Ana López-Yela, Yi Huang, *Senior Member, IEEE*, Daniel Segovia-Vargas, *Member, IEEE*, Yuan Zhuang, Yansong Wang and Jiafeng Zhou

Abstract—There has been an increasing demand for smart devices and smart furniture for home automation, monitoring and security applications. In this paper, we present a novel method of integrating the function of wireless energy harvesting from ambient RF signals to a conventional quartz clock for home applications. The most attractive feature is that the clock itself is used as the power receiving device, thus no additional antennas are needed. A simple rectifier is designed to directly match with the clock antenna and rectify the power captured by the clock. As a design example, a clock rectenna using the proposed new idea achieves good energy conversion efficiency (up to 65%) over its operating frequency bands at around 1.4 – 1.5, 1.9 – 2.1 and 2.4 – 2.8 GHz respectively. Moreover, a wireless environmental sensor is integrated with the clock and powered by using the harvested power from the proposed clock rectenna. This novel design greatly expands the functionality of the quartz clock without affecting its size and appearance. We believe that the proposed energy harvesting quartz clock could be adopted for smart home applications.

Index Terms—Clock, rectenna, smart home, wireless energy harvesting, wireless sensors;

I. INTRODUCTION

SMART devices and smart furniture for home applications have attracted significant interests in the past decades. For example, Google launched their Google Home smart speaker and electriQ Smart Lighting dimmable color WiFi bulb in 2016 and 2017 respectively, which has gained a lot of attention [1]. The function of artificial intelligence has been embedded into these smart devices for assisted living that is based on a wireless sensor network (WSN) [2]. Consequently, many wireless sensors (e.g., environmental and motion sensors) have been applied in the design of the aforementioned smart devices

and smart furniture, which enables a range of smart home applications in such as building automation, environmental monitoring and home security etc. [3]–[5]. Moreover, the application of these wireless sensors is of great importance to the development of the Internet of Things (IoT) [6].

However, there are still a number of major challenges. One is the battery replacement for these wireless sensing applications. To overcome this problem, ambient energy harvesting from different sources (e.g., solar, vibration, thermal, wind and RF energies) has been identified as an appropriate solution for powering these wireless sensors [7]–[9]. Among all sources, RF energy sources are becoming increasingly popular since they are ubiquitously available (i.e. from ambient Digital TV, cellular mobile network and WiFi signals) in most domestic environments regardless of the time, weather and environmental conditions [10]. However, the electromagnetic energy captured from these wireless signals is normally lower than 1 mW due to the limits of RF radiation [11]. As a consequence, the ambient wireless energy harvesting technology might only be suitable for low power wireless sensing applications at present [12].

Many different types of rectifying antennas (rectennas) have been developed for wireless energy harvesting applications [13]–[17]. Multiband and broadband rectennas and their arrays could normally harvest sufficient energy to power the aforementioned sensors [18]–[22]. But, their antenna size is normally quite large and the circuit structure is also very complex. Thus, such wideband rectennas may be not suitable for some indoor miniaturized small sensors.

In this paper, we present a novel method of adding the wireless energy harvesting and wireless sensing functions to a quartz clock, which is one of the most popular home furniture. Different from existing wireless rectenna designs for clocks and motors [23]–[25], the most distinguishable feature of this work is that the clock itself is used as the power receiving antenna. The complete clock rectenna is realized by adding a simple rectifier without the need of extra antennas and matching circuits. In addition, a small wireless environmental sensor is introduced to the clock and powered using the energy captured by the clock rectenna. These modifications will not affect the size and appearance of the clock, but they have definitely made such a quartz clock “smart” for a range of smart home and IoT applications.

The rest of this paper is organized as follows. Section II presents the structural analysis of the quartz clock. Section III

Manuscript received December 18, 2017, revised March 06, 2018 and April 23, 2018, accepted May 27, 2018. This work was supported in part by the EPSRC, U.K., and in part by the Spanish Ministry of Education, Culture and Sport under a grant for pre-doctoral contracts for University Teacher Training (FPU). A. López-Yela's work was supported by University Carlos III of Madrid (UC3M) Scholarship for pre-doctoral students. (*Corresponding authors: Daniel Segovia-Vargas and Yi Huang*).

C. Song, Y. Huang, Z. Yuan, Y. Wang and J. Zhou are with the Department of Electrical Engineering and Electronics, University of Liverpool, Liverpool L69 3GJ, U.K. (e-mail: chaoyun.song@liv.ac.uk; yi.huang@liv.ac.uk).

A. López-Yela and D. Segovia-Vargas are with the Departamento de Teoría de la Señal y Comunicaciones, Universidad Carlos III de Madrid, 28911 Leganés, Spain. (e-mail: anlopezy@ing.uc3m.es; dansevar@ing.uc3m.es).

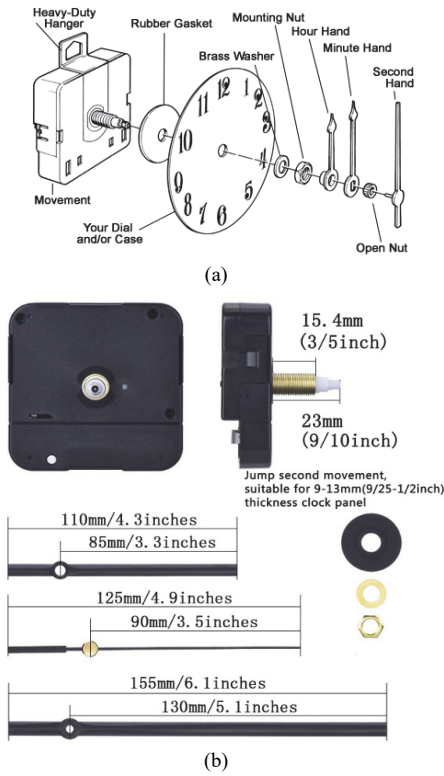


Fig. 1. (a) The disassembled drawing of a typical quartz clock product. (b) The picture of an example of a real quartz clock product for home applications (reproduced with the permission of Woodworking Parts [26]).

shows the detailed description of the wireless energy harvesting clock rectenna design. The wireless sensor integration and its performance evaluation is introduced in Section IV. Finally, the performance comparison is given in Section V and conclusions are drawn in Section VI.

II. STRUCTURAL ANALYSIS OF QUARTZ CLOCK

A quartz clock is a clock that utilizes an electronic oscillator which is regulated by a quartz crystal to keep time. The crystal oscillator creates a signal with a very precise frequency, so that the quartz clocks are at least an order of magnitude more accurate than mechanical clocks. The first quartz clock was built by Warren Harrison and J. W. Horton at Bell Telephone Laboratories in 1927 [27]. Nowadays, quartz clock products have become essential equipment in our daily life. They have either been beautifully embedded into home furniture (e.g., a wall mounted clock), or been developed to a wrist watch. According to the annual report of Cartier, a French luxury goods company which designs, manufactures, and sells jewelry and watches, the sales in the watch market have produced a revenue of 1.2 billion US dollars in 2017, which is equivalent to 22% of their annual income. This demonstrates that there is still a huge demand for quartz clock products in the 21st century.

Generally, a quartz clock consists of three major parts, namely, a clock movement mechanism, a clock face (dial) and three clock hands. Fig. 1 (a) shows a disassembled drawing of a typical quartz clock. In addition to the aforementioned three parts, there are other installation accessories such as the rubber gasket, mounting nuts and brass washer. The picture of a real

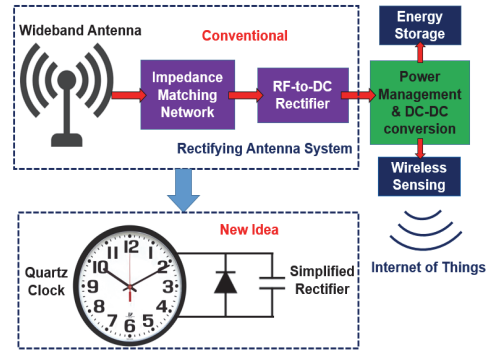


Fig. 2. The block diagram illustration of using the proposed new energy harvesting quartz clock to substitute the conventional rectifying antenna system and their applications in energy storage and wireless sensing.

product of the quartz clock (exclude the clock dial) is given in Fig. 1 (b) with detailed dimensions. The size of the clock movement mechanism is about $56 \times 56 \times 15 \text{ mm}^3$. The crystal oscillator, circuit board and battery are disposed inside this movement mechanism. The spindle for controlling the clock hands is about 23 mm in height, and 3 mm in radius while the outer shaft for the installations of gasket, dial and nuts is about 15 mm in height. The lengths of clock hands for hour, minute and second are about 110, 155 and 125 mm respectively. It is worth noting that, this dimension example represents a typical size of the quartz clock product for home applications.

In terms of material, the clock hands are normally made by aluminum while the shaft and inner spindle are made by copper. This feature improves the robustness and durability of the product. Additionally, the quartz clock products are usually of a very low power consumption, typically around 5-60 μW , which is smaller than that of some digital clocks with a LCD display. The battery life of the quartz clock depends on a number of facts such as the clock size.

By integrating the function of ambient energy harvesting (e.g., from solar, piezoelectric and RF energies etc.) to such quartz clock products, their battery life-span can be significantly extended which may eliminate the need of the battery replacement in principle. However, most of these energy harvesting functions requiring additional devices with a certain size (e.g., solar panels and piezoelectric materials) to capture energy. As a drawback, it will increase the cost of products and meanwhile affect their appearances.

Here we will introduce a novel method of integrating a low-cost and simple wireless energy harvesting module on the aforementioned quartz clock products. The clock itself will be used as the harvesting device to capture energy from ambient electromagnetic fields (e.g., cellular mobile and WiFi); thus, no additional antennas are needed for the complete product design.

III. WIRELESS ENERGY HARVESTING INTEGRATION

Ambient wireless energy harvesting (AWEH) from existing electromagnetic fields is an emerging technology. The rectenna system is the most crucial device for AWEH applications. Fig. 2 depicts the block diagram of a typical rectenna system that consists of a wideband receiving antenna, an impedance matching network and an RF-to-DC rectifier, and also shows its application in energy storage and wireless sensing applications.

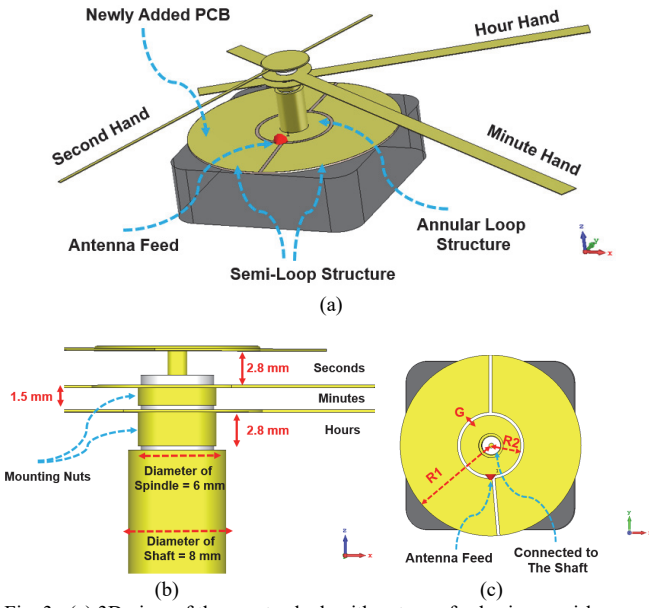


Fig. 3. (a) 3D view of the quartz clock with antenna feed using semi-loop and annular loop structures on a PCB. (b) Side view of the clock spindle and clock hands. (c) Top view of the PCB.

The broadband antenna in such a system is normally of a large size in order to cover a wide signal spectrum and capture sufficient power from these ambient wireless signals.

Furthermore, the circuit topology of the impedance matching network (which is aimed at getting the complex input impedance of the rectifier matched to a standard 50-ohm) for such a broadband rectenna system is normally very complex [19]. Therefore, the aforementioned conventional broadband rectennas using a relatively large antenna and complex circuitry are not suitable for the proposed quartz clock products. A need exists for an innovative and effective method for the integration between the rectenna and clock.

Based on the structural analysis of a typical quartz clock as discussed in Section II, it is found that the dimensions of the metal parts (e.g., spindle, shaft, and clock hands) are almost fixed for different clock products. If these metal parts could be utilized wisely, the clock itself could be regarded as an antenna without the need of adding additional radiating elements. Moreover, it is also found that the dimensions of the clock hands are electrically large enough (compared with the wavelength) to cover the majority of existing RF bands such as GSM 900, 1800, UTMS2100 and ISM 2.45 GHz. In this way, we could eliminate the need of a large wideband receiving antenna for the rectenna system as given in Fig. 2. Furthermore, by using the latest technology of inherent impedance matching between the rectifier and antenna [28], we could also get rid of the complex impedance matching network. Consequently, the AWEH function could be effectively integrated to the quartz clock products by feeding the clock using a simple rectifier (as depicted in Fig. 2).

The harvested power could be used either to extend the battery life of the clock or to power wireless sensors (e.g., temperature and humidity sensors) which may expand the functionality of the quartz clock.

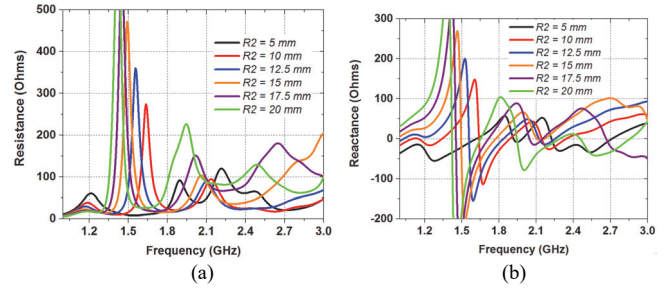


Fig. 4. Simulated (a) resistance and (b) reactance of the proposed clock antenna with different values of R_2 .

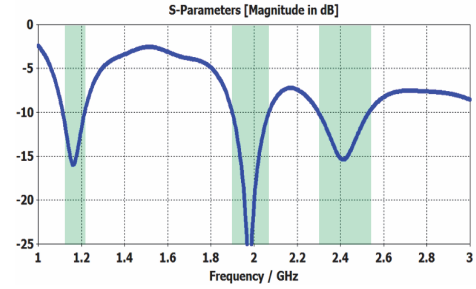


Fig. 5. Example of simulated reflection coefficient of the clock antenna for $R_2 = 5$ mm and using 50 Ω port impedance.

A. Using Clock as an Antenna

Based on the product drawing and dimensions of the quartz clock as depicted in Fig. 1, the 3D model of the clock is built using the Computer Simulation Technology (CST) software. As shown in Fig. 3 (a), the metal parts such as the clock spindle and clock hands are modelled using a perfect electric conductor (PEC) with a yellow colour. The black box underneath these metal parts represents the clock movement mechanism. There is a newly added printed circuit board (PCB) disposed on the movement mechanism, which is the key component to feed the entire clock as an antenna. The PCB fabrication technology is suitable for RF circuits that consists of surface-mount devices (SMD). Other fabrication technologies (e.g., inkjet printing [18]) using flexible substrates could also be considered for making the rectifier. But the PCB technology has advantages in terms of manufacturing simplicity and low cost.

The PCB is single-sided, while the top circuit consists of an annular loop structure and two semi-loop structures. The annular loop is electrically connected to the cooper shaft of the clock spindle. When a signal excitation port is differentially fed between the annular loop and a semi-loop structure, the entire clock can be regarded as a quasi-dipole-type antenna. The first pole is the shaft and the annular loop while the second pole is the semi-loop. Moreover, the clock hands are coupled to the shaft with a small gap, which could also be used as the radiating elements. The enlarged side view of the clock spindle and clock hands is given in Fig. 3 (b). It can be seen that the distance between the hour hand and spindle is 3 mm while the height of the mounting nut is about 2.8 mm. The separation between the minute and hour hand is about 1.7 mm while the height of the mounting nut is 1.5 mm.

Fig. 3 (c) shows the top view of the PCB. The outer radius of the annular loop and the radius of the complete board are represented using R_2 and R_1 respectively. The gap between the annular loop and the semi-loop is G . The value of G is set as 1

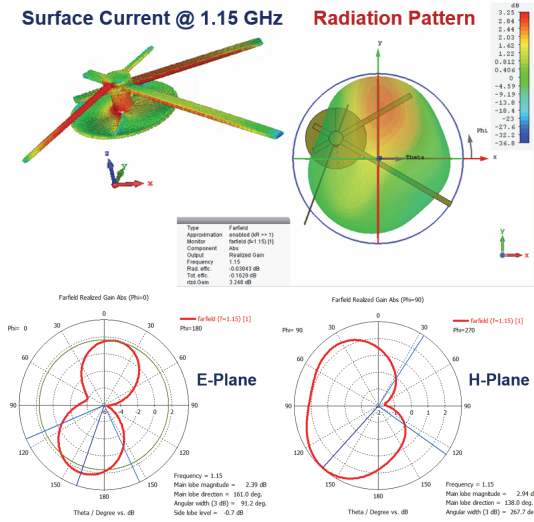


Fig. 6. The simulated surface current distribution and 3D radiation pattern of the clock antenna using 50 Ω port impedance and $R_2 = 5$ mm at 1.15 GHz. The corresponding 2D patterns over the E-plane (elevation plane) and H-plane (azimuth plane) are shown as well.

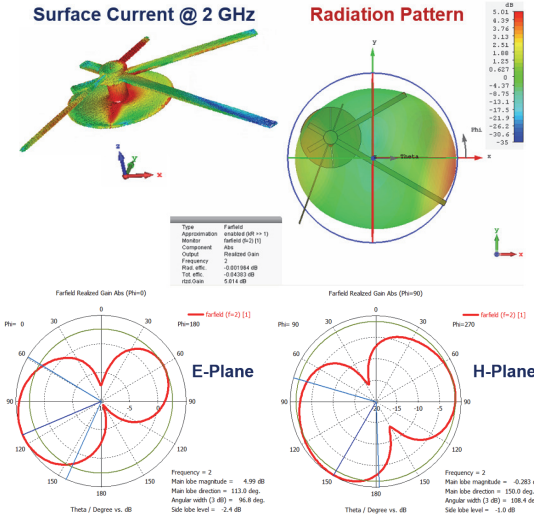


Fig. 7. The simulated surface current distribution and 3D radiation pattern of the clock antenna using 50 Ω port impedance and $R_2 = 5$ mm at 2 GHz. The corresponding 2D patterns over the E-plane (elevation plane) and H-plane (azimuth plane) are shown as well.

mm in this work in order to configure the rectifying diodes. The value of R_1 is 30 mm. Thus the size of the PCB (diameter = 60 mm) is similar to that of the movement mechanism. The substrate material of the PCB is Duroid5880 with a relative permittivity of 2.2, a loss tangent of 0.0009 and a thickness of 0.51 mm. Consequently, the addition of this small piece of PCB would not increase the size and weight of the quartz clock products significantly. It will also not affect the appearance of the product when the clock dial is installed. Fig. 4 depicts the simulated input impedance of the complete clock antenna as shown in Fig. 3 (a). The value of R_2 is swept between 5 and 20 mm in order to analyse its effect on antenna resonant frequencies. It can be seen that the proposed clock antenna has three major resonant frequencies ranging between 1 to 3 GHz for the value of R_2 varies from 5 to 20 mm. An example of the simulated reflection coefficient (S_{11}) of the clock antenna using

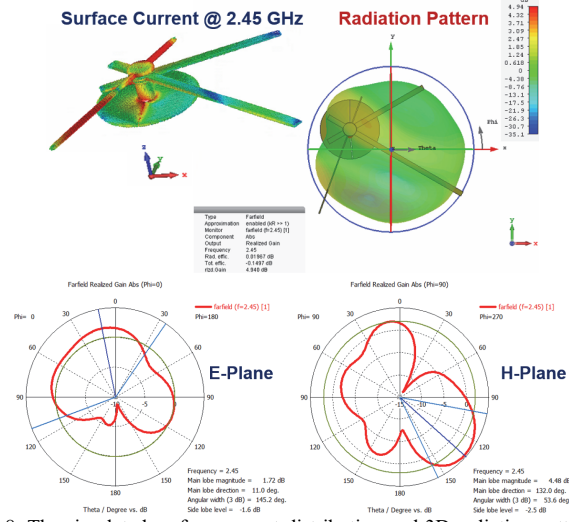


Fig. 8. The simulated surface current distribution and 3D radiation pattern of the clock antenna using 50 Ω port impedance and $R_2 = 5$ mm at 2.45 GHz. The corresponding 2D patterns over the E-plane (elevation plane) and H-plane (azimuth plane) are shown as well.

a standard 50 Ω port impedance is given in Fig. 5 for $R_2 = 5$ mm. The resonant frequency bands in this case for $S_{11} < -10$ dB are 1.1 – 1.2, 1.9 – 2.08, and 2.3 – 2.55 GHz respectively.

In addition, in order to understand the operation mechanism of this clock antenna, the surface current distributions and radiation patterns for the design example using 50 Ω port impedance and $R_2 = 5$ mm are depicted in Figs. 6-8 at three different frequencies. It can be seen that the dominant currents at 1.15 GHz are located at the shaft, second hand and hour hand of the clock, which produces a maximum antenna beam towards the direction of the hour hand with a realized gain of 3.2 dBi (see Fig. 6). While the maximum radiation beam of the antenna is tilted to the direction of the minute hand at 2 GHz, as can be seen from the 3D and 2D patterns in Fig. 7. The realized gain in this case is about 5 dBi. The surface currents are the strongest on the second hand at 2.45 GHz. Such current distributions switch the radiation beam of the clock antenna to the direction of the second hand. From Fig. 8, it is shown that the realized gain at 2.45 GHz is of around 4.9 dBi. The above results demonstrate that the typical quartz clock can be used as a quasi-dipole-type antenna with the aid of a simple feed structure on the PCB. Also, it is noted that this modification will not affect the normal function of the clock, while the resonant frequency of the clock antenna might be relatively stable, irrespective of the rotation of clock hands. This is due to the coupled radiating elements (clock hands) and their fixed electrical length. The antenna beam directions could be steered by the movement of clock hands during the time keeping.

This feature may also be advantageous for the proposed WEH application due to the arbitrary incoming waves from unknown directions in a realistic ambient environment.

B. Rectifier Configuration

By integrating a rectifier on the feed port of the clock antenna, the received RF power by the clock antenna could be rectified into DC power. For simplicity, the impedance matching network will not be used in the rectifier design as mentioned

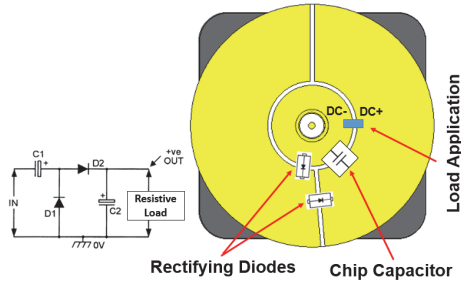


Fig. 9. Configuration of the simplified rectifier on the PCB and its equivalent circuit model.

TABLE I
INPUT IMPEDANCE OF THE PROPOSED RECTIFIER

	Freq. (GHz)	Input Power = -10 dBm	Input Power = 0 dBm	Input Power = +10 dBm
Load Resistance = 500 Ω	1.2	230 -j60 Ω	161 -j26 Ω	132 -j10 Ω
	1.4	200 -j63 Ω	152 -j30 Ω	132 -j11 Ω
	1.6	176 -j65 Ω	143 -j33 Ω	129 -j13 Ω
	1.8	156 -j66 Ω	134 -j36 Ω	127 -j14 Ω
	2	140 -j67 Ω	125 -j38 Ω	123 -j17 Ω
	2.2	126 -j68 Ω	117 -j40 Ω	118 -j20 Ω
	2.4	114 -j69 Ω	111 -j41 Ω	113 -j21 Ω
Load Resistance = 1000 Ω	1.2	241 -j66 Ω	211 -j40 Ω	203 -j20 Ω
	1.4	208 -j68 Ω	193 -j44 Ω	195 -j24 Ω
	1.6	182 -j70 Ω	176 -j47 Ω	187 -j28 Ω
	1.8	161 -j71 Ω	160 -j50 Ω	177 -j32 Ω
	2	143 -j72 Ω	147 -j52 Ω	167 -j35 Ω
	2.2	128 -j73 Ω	135 -j54 Ω	157 -j37 Ω
	2.4	115 -j74 Ω	134 -j55 Ω	140 -j41 Ω
Load Resistance = 2000 Ω	1.2	251 -j72 Ω	241 -j48 Ω	244 -j33 Ω
	1.4	215 -j74 Ω	215 -j52 Ω	227 -j38 Ω
	1.6	187 -j75 Ω	193 -j56 Ω	210 -j42 Ω
	1.8	164 -j76 Ω	174 -j58 Ω	194 -j45 Ω
	2	146 -j77 Ω	163 -j65 Ω	179 -j48 Ω
	2.2	131 -j78 Ω	147 -j66 Ω	166 -j50 Ω
	2.4	118 -j78 Ω	134 -j67 Ω	153 -j52 Ω

earlier. As a consequence, an in-depth investigation on the input impedance of the rectifier is required in order to find the optimal antenna impedance for inherent complex conjugate impedance matching between the antenna and the rectifier.

The rectifier configuration on the PCB of the clock antenna is shown in Fig. 9. There are only two rectifying diodes used in the design. The first diode is mounted between the annular loop and the first semi-loop while the second diode is mounted between the two semi-loop structures. Additionally, a chip capacitor is used for energy storage and output smoothing. The equivalent circuit model of this rectifier is shown as well, which is a typical model of the voltage doubler rectifying circuit. It is noted that the series capacitor $C1$ in the equivalent circuit could be eliminated for such a differentially fed dipole-type rectifying antenna structure [29].

The rectifier is simulated using the Advanced Design System (ADS) software. As an example, a Schottky diode HSMS2850 is used as the rectifying diodes. The diode is modelled using the

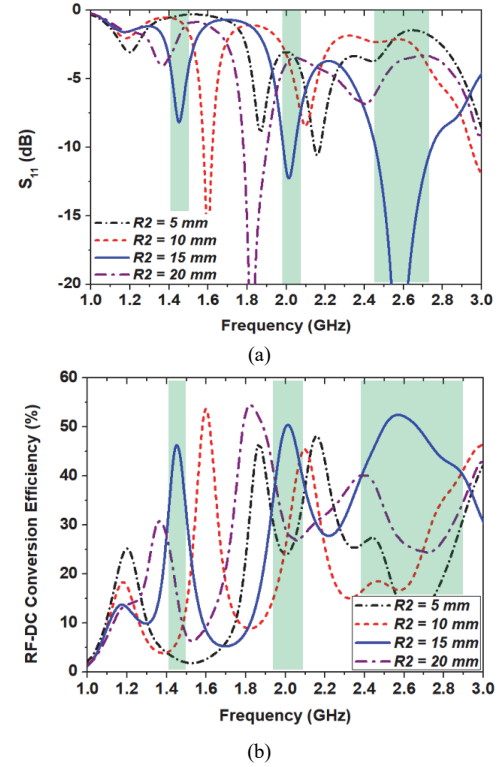


Fig. 10. The simulated (a) reflection coefficient and (b) RF-DC conversion efficiency of the complete clock rectenna. Note that the diodes are HSMS2850, chip capacitor is 100 nF, input power is 0 dBm and load resistance is 1000 Ω .

real product model (by taking the parasitic element and packaging effect into account) provided by Avago. The chip capacitor is a 100 nF SMD capacitor from Murata. The Large Signal S-parameter (LSSP) and Harmonic Balance (HB) simulations are used to analyse the input impedance of the rectifier structure as depicted in Fig. 9. The results of the rectifier impedance are given in Table I for three different input power levels and load resistance values. Due to the nonlinearity of the rectifier, the input impedance of the rectifier is normally a function of frequency, power and load. From Table I, it can be seen that the real part of the impedance (resistance) varies between 230 and 118 Ω over the frequency band of 1.2 – 2.4 GHz, input powers between -10 and 10 dBm, and load resistance from 500 to 2000 Ω . While the imaginary part of the impedance (reactance) is of negative values, which varies between -78 and -10 Ω for the aforementioned conditions. Since the clock antenna impedance for different feed locations (values of $R2$) has been presented in Fig. 4, we could select the optimal antenna design which shows the best impedance matching performance in accordance with the rectifier impedance as depicted in Table I. In this way, the complete rectenna design may not need additional impedance matching circuits which simplifies its structure and reduces the cost.

C. Clock Rectenna Performance Evaluation

According to the results of the clock antenna impedance as depicted in Fig. 4, the performance (e.g., impedance matching, conversion efficiency and output voltage etc.) of the complete

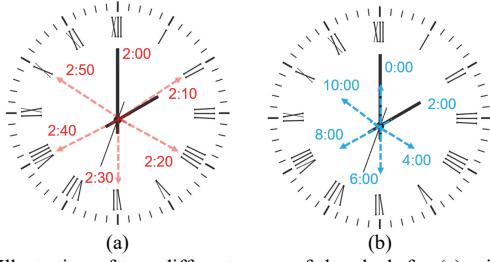


Fig. 11. Illustration of two different cases of the clock for (a) minute hand rotates from 2:00 to 2:50 and (b) hour hand rotates from 0:00 to 10:00.

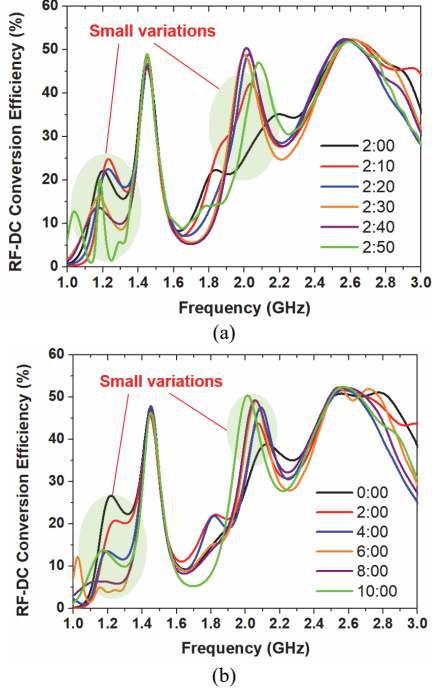


Fig. 12. The simulated RF-DC conversion efficiency of the complete clock rectenna ($R_2 = 15$ mm) for (a) minute hand rotates from 2:00 to 2:50 and (b) hour hand rotates from 0:00 to 10:00. The input power is 0 dBm and load resistance is 1000 Ω .

quartz clock rectenna could be estimated. Firstly, a frequency domain power source was used for the rectifier simulation. The default port impedance (50 Ω) could be changed to the frequency-dependent complex impedance of the clock antenna. To achieve this, a file-based touchstone file was exported from the CST for the antenna impedance. Then, the Data Access Component (DAC) of the ADS was employed to load this file for the port impedance of the rectifier. When the rectifier model was simulated, the imported clock antenna impedance was also used at the same time. Therefore, the complete clock rectenna was co-simulated using the CST and ADS software.

The simulated S_{11} and RF-DC conversion efficiency of the complete clock rectenna are given in Fig. 10 versus the frequency band of interest. Note that the input power and load resistance here are 0 dBm and 1000 Ω as an example. The RF-DC conversion efficiency is calculated using

$$\eta_{RF-DC} = \frac{P_{DC}}{P_{in}} \quad (1)$$

where P_{in} is the input RF power to the rectifier, P_{DC} is the output DC power that can be obtained using $P_{DC} = V_{DC}^2/R_L$, where V_{DC} is the output voltage and R_L is the load resistance.

Moreover, to identify the optimal clock antenna design, the results for different values of R_2 (from 5 to 20 mm) are also presented in Fig. 10. It can be found that the best impedance matching performance is obtained when $R_2 = 15$ mm, because the S_{11} is smaller than -10 dB at the frequency bands around 2.1 and 2.45 GHz which covers the UMTS2100 and ISM bands. In this scenario, the RF-DC conversion efficiency of this design example is above 40% over the frequency bands of 1.4 – 1.5, 1.9 – 2.1, and 2.4 – 2.9 GHz. It is demonstrated that the feed position at $R_2 = 15$ mm is the optimal location for getting the impedance of the clock antenna and rectifier matched over the frequency band of interest.

Another interesting study here is to analyze the performance variation (e.g., impedance matching and conversion efficiency) of the clock rectenna when the clock hands are moving over time. As given in Figs. 11 (a) and (b), two groups of clock hand scenarios are investigated herein, which are:

- 1) Minute hand of the clock rotates for 50 minutes, from 2:00 to 2:50 with a step of 10 minutes.
- 2) Hour hand of the clock rotates for 10 hours, from 0:00 to 10:00 with a step of 2 hours.

These cases may include the majority of the clock hand scenarios. The antenna impedance of the proposed clock under the aforementioned cases is first analyzed using the CST EM simulation, which is similar to the process of getting the results of Fig. 4. Afterwards, the antenna impedance is utilized to obtain the RF-DC power conversion efficiency of the rectenna with the aid of the ADS software. The detailed approach of this step is identical to the method of getting the results in Fig. 10 (b). Finally, the simulated conversion efficiency of the complete clock rectenna for the two groups of clock hand cases is depicted in Fig. 12. To compare with the results of Fig. 10 (b), the input power and load resistance here are set as 0 dBm and 1000 Ω . From Fig. 12, it can be seen that, the conversion efficiency is slightly changed for different cases at around 1 – 1.2 GHz and 2 GHz. This is due to the impedance variation of the clock antenna over the time. The minute hand has an impact on the performance at 2 GHz while the performance at 1.2 GHz is more dependent on the condition of the hour hand. The efficiency at the bands of 1.4 – 1.5 and 2.2 – 2.8 GHz is relatively stable, which means that impact on performance due to the antenna impedance variation is relatively small.

Having selected the optimal feed location ($R_2 = 15$ mm) for the proposed rectenna, the clock rectenna prototype is fabricated and tested. As shown in Fig. 13 (a), the rectifier is integrated on the PCB that is placed over the clock movement mechanism. Other parts of the clock have not been modified. Fig. 13 (b) depicts the measurement setup of the clock rectenna example, where the signals generated by an RF signal generator were amplified by a 30-dB gain power amplifier (PA), and transmitted by a calibrated horn antenna R&SHF906. The proposed clock rectenna was used to receive the signal at a distance of 1 m from the transmitting horn antenna. The transmitting power was measured by a power meter while the received power by the rectenna was calculated by using the Friis transmission equation

$$P_r = P_t + G_t + G_r + 20 \log_{10} \frac{\lambda}{4\pi r} \quad (2)$$

where P_r is the input RF power to the rectifier in dBm, P_t is the transmitting power of the horn in dBm, G_t is the realized gain of

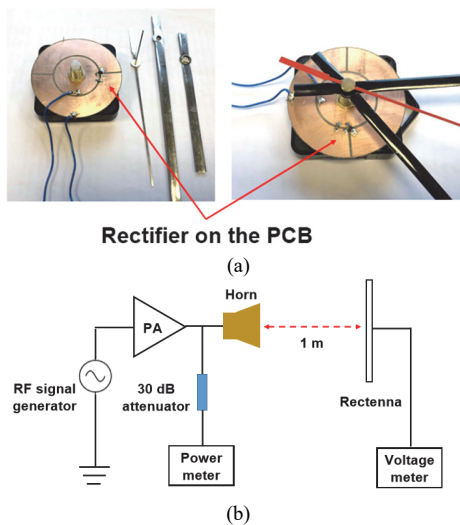


Fig. 13. (a) The fabricated clock rectenna example with and without the installation of clock hands. (b) Measurement setup of the clock rectenna. The rectenna orientation was tuned for the maximum output DC voltage during the measurement.

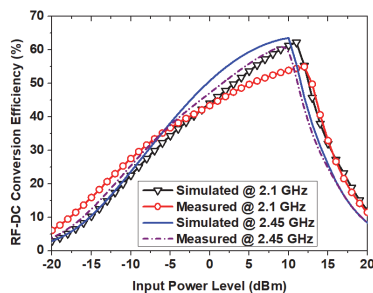


Fig. 14. The measured and simulated RF-DC conversion efficiency at two frequencies vs. input power level of the fabricated clock rectenna prototype. Note that the diodes are HSMS2850, chip capacitor is 100 nF, and load resistance is 1000 Ω .

the horn in dBi, G_r is the realized gain of the proposed rectenna in dBi, λ is the wavelength of interest, and r is the distance ($r = 1$ m). It is noted that the antenna orientation at each frequency band was tuned to match with its maximum beam direction during the measurement (in order to avoid additional power loss). This can be achieved by recording the orientation that produced the highest output DC voltage of the rectenna. Since the antenna has been integrated with the rectifier, the realized gain of the clock rectenna cannot be measured with a typical 50 Ω port. To calculate the realized gain, the directivity of the clock antenna was first used to multiply its radiation efficiency. Both parameter can be obtained from the far-field results using the CST. The next step was to use this calculated antenna gain to multiply the impedance matching efficiency of the complete clock rectenna. The matching efficiency was calculated using the LSSP simulator of the ADS. This will take the impedance mismatch between the antenna and rectifier into account, thus producing an accurate estimation for the realized gain.

The results of conversion efficiency vs. input power using the aforementioned clock rectenna design are provided in Fig. 14 at two frequencies. A 1000 Ω load resistor is used here to obtain these results. The peak efficiency is around 65% at 10 dBm input power. While the efficiency is above 50% for input power varying between 0 and 12 dBm. The measured and simulated conversion efficiency versus frequency are given in

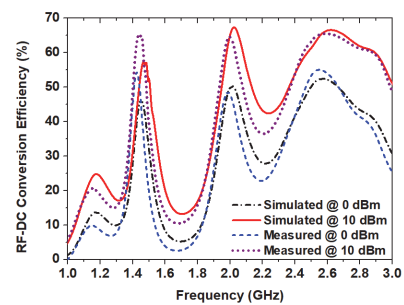


Fig. 15. The measured and simulated RF-DC conversion efficiency at two input powers vs. frequency of the fabricated clock rectenna prototype. Note that the diodes are HSMS2850, chip capacitor is 100 nF, and load resistance is 1000 Ω .

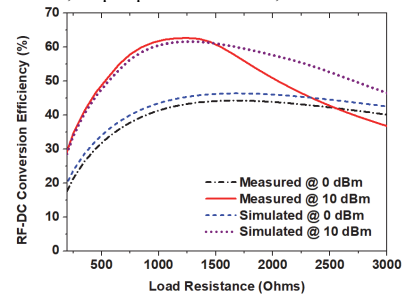


Fig. 16. The measured and simulated RF-DC conversion efficiency at two input powers vs. load resistance of the fabricated clock rectenna prototype. Note that the diodes are HSMS2850, chip capacitor is 100 nF, and frequency is 2.45 GHz.

Fig. 15 at the input power of 0 and 10 dBm respectively. It can be seen that the frequency bands for the optimal efficiency is around 1.4 – 1.5, 1.9 – 2.1 and 2.4 – 2.8 GHz respectively. Moreover, the efficiency versus load resistance at these two input power levels are shown in Fig. 16 at 2.45 GHz. The conversion efficiency is relatively stable over the load resistance from 500 to 3000 Ω .

The above results show that the proposed clock rectenna has achieved good performance without using additional antennas and impedance matching networks. The performance of the proposed clock rectenna is comparable to that of many existing wideband and multiband rectennas. It is demonstrated that the AWEH function has been effectively integrated to the clock.

IV. WIRELESS SENSING FUNCTION INTEGRATION

To utilize the harvested power of the clock rectenna, a power management unit (PMU) with a DC-DC boost converter is needed since the output voltage from the rectenna is normally lower than the usable voltage level (e.g., 3 V). Here we employ an ultra-low-power boost converter with a battery management (from Texas Instrument [30]) for the proposed design. Fig. 17 depicts the schematic diagram of this PMU and its configuration with the proposed clock rectenna. It is noted that the cold-start voltage and quiescent current of the PMU are 0.33 V and 330 nA respectively. The minimum input voltage is down to 0.1 V while the DC-DC conversion efficiency is maintained over 75% (up to 90%) for the input voltage between 0.6 and 3 V. The output voltage is eventually regulated to 3.3 V for battery charging and other load applications.

The measured output voltage of the clock rectenna and PMU versus the input RF power to the rectifier is given in Fig. 18. Note that the output voltage of the clock rectenna is identical to

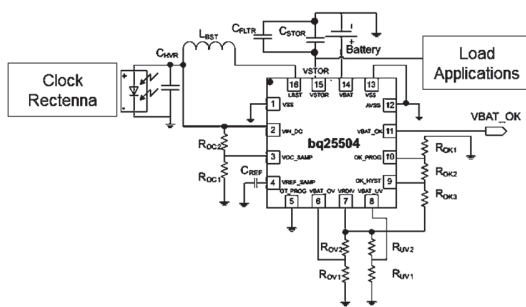


Fig. 17. Schematic of a BQ25504 power management unit, a DC-DC boost converter and the configuration with the proposed clock rectenna.

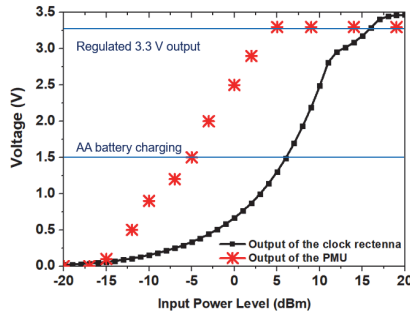


Fig. 18. Measured output voltage of the clock rectenna and the PMU vs. input RF power to the rectifier. The input voltage to the PMU is identical to the output voltage of the rectenna.

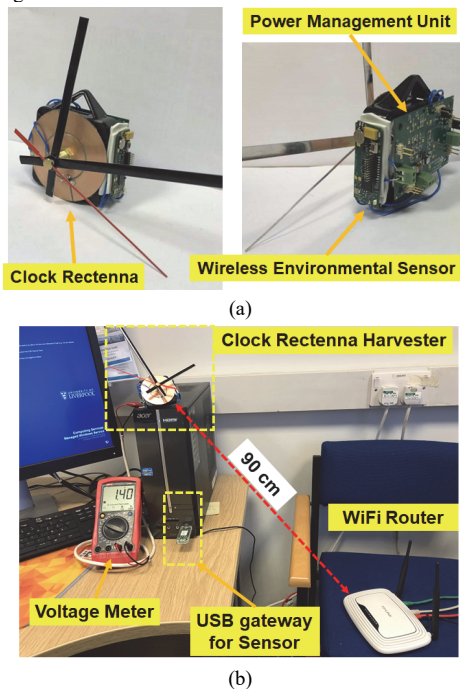


Fig. 19. (a) The complete clock rectenna with the configuration of PMU and a wireless environmental sensor. (b) The real application example of using the clock antenna to harvest energy from a typical WiFi router at a distance of 0.9 m. The harvested power is used to power the wireless sensor which sends data to the cloud via a USB gateway.

the input voltage of the PMU. It can be seen that PMU starts to operate at the input power of -15 dBm. While the output voltage reaches 1.5 V for -5 dBm RF input, which is sufficient for charging an AA battery. The input voltage of the PMU is about 0.5 V in this scenario. Moreover, when the input RF power is 5 dBm, the output voltage of the clock rectenna is 1.3 V and

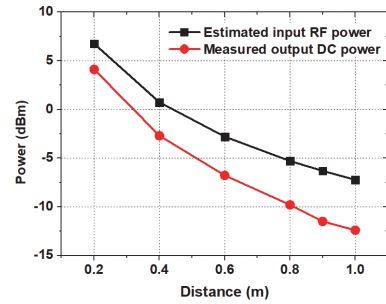


Fig. 20. The estimated input RF power to the rectifier and measured output DC power from the clock rectenna versus the distance between the clock rectenna and WiFi router.

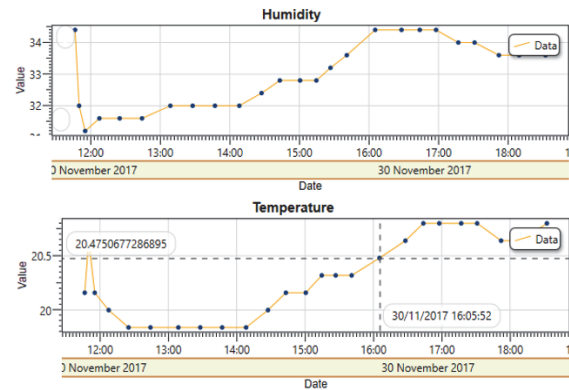


Fig. 21. The data monitoring of the sensor using Dolphin View software [32]. The sensor payload, RSSI, and data transmission interval are shown as well.

meanwhile the output voltage of the PMU reaches its saturation level, which is 3.3 V as mentioned above. This voltage level is suitable for many wireless sensors. Therefore, the wireless sensing could be integrated with the clock rectenna, and powered by using the harvested power.

As a demonstration, a low power wireless environmental sensor from EnOcean Technology [31] is employed in the proposed design. The sensor could measure the temperature and humidity data and transmit the data via an 868 MHz long-range (up to 50 meters) wireless radio link. The transmitting power of the sensor is of around 5 dBm, while the data could be received using a USB sensor gateway with a minimum sensitivity of -100 dBm. The operating power consumption of the sensor is about 8 μ W and its start-up voltage is 1.5 V. The design example of the complete clock rectenna integrated with the PMU and the wireless sensor is given in Fig. 19(a). The output power from the PMU is used to power the sensor directly. The harvested power is also used to charge a small battery for supporting sensor data transmissions. The application demonstration of the proposed wireless powered clock rectenna and its wireless sensing function are depicted in Fig. 19 (b). It can be seen that the clock rectenna captured energy from a typical 2.45 GHz WiFi router (TP Link TL-WR841N) over a distance of 0.9 m. The router was used in a typical office area (around 30 m^2) which has 16 desktops and

TABLE II
PERFORMANCE COMPARISON WITH RELATED DESIGNS

	This work (2018)	[23] (2017)	[24] (2007)	[25] (2008)	[13] (2017)	[18] (2018)	[22] (2015)	[28] (2017)
Extra receiving antenna	NO	YES	YES	YES	YES	YES	YES	YES
Impedance matching networks	NO	YES	YES	YES	YES	YES	YES	NO
Frequency bands (GHz)	1.4 – 1.5, 1.9 – 2.1, 2.4 – 2.8	2.4 – 2.5	2.45	2.45	1.75 – 1.85	0.79 – 0.96, 1.71 – 2.69	1.8 – 2.5	0.9 – 1.1, 1.8 – 2.5
Maximum conversion efficiency	65%	60%	52%	70%	61%	57%	70%	75%
Optimal power (Efficiency > 40%)	-5 to 15 dBm	Not reported	Not reported	Not reported	-15 to 10 dBm	-5 to 10 dBm	-20 to 0 dBm	-5 to 15 dBm
Complexity of the overall design	Very simple	Complex	Simple	Complex	Complex	Complex	Very complex	Simple
Load applications and devices	Clock, wireless sensors	Humidity sensor	Clock	Clock and DC motor	Digital watch	Not reported	Not reported	Not reported

9 mobile devices and laptops. The experiment was conducted during the week days in which the office was almost fully occupied. Since the radiating power of this WiFi router was around 0.1 W (20 dBm) while the router used two omnidirectional 5 dBi sleeve dipole antennas, the received power by the clock rectenna and the input RF power to the rectifier can be estimated using the free space path loss equation as given in (2). As a result, the estimated input RF power to the rectifier is obtained as a function of the distance between the clock rectenna and the WiFi router (see Fig. 20). The corresponding measured output DC power is also presented in this figure. It can be seen that the input RF power to the rectifier at the distance of 0.8 m is about -5 dBm. According to the results in Fig. 14, the conversion efficiency in this case is around 35%, which results in a rectified DC power of -9.6 dBm (the measured value was -9.9 dBm). The harvested power of the clock rectenna is higher than -12.5 dBm (56 μ W) for the distance to the router within 1 m.

Fig. 21 shows the data monitoring of the sensor using the Dolphin View software. The real-time values of temperature and humidity are shown in the charts against the time. In the bottom part of the figure, the payload data, relative received signal strength (RSSI) and data transmission interval of the sensor are provided as well. It can be seen that, using the captured energy from the clock rectenna at a distance of 0.9 m to the WiFi router, the wireless sensor could send data in every 15–20 minutes, which is sufficient for such an indoor environmental monitoring application. According to Fig. 20, when the distance between the clock and the router is further increased, the harvested DC power could be lower than -20 dBm. In this scenario, the sensor needs to accumulate enough energy for the data transmission, thus the sensor data transmission interval has to be increased to 60 – 80 minutes. It should be noted that the WiFi router is just an example of the typical RF power sources. Recently, *Energous* has launched the first commercially available far-field RF power transmitters that could deliver more power and achieve efficient wireless energy harvesting at a longer distance [35].

It is noted that the clock rectenna here is optimized for the input power above -10 dBm, which is higher than the typical ambient RF signal levels (e.g., around -30 dBm). The reason

here was to ensure that enough power could be harvested for experimental validation purposes. When the rectifying diodes of this design are changed to very low power diodes (e.g., heterojunction backward tunnel diodes [36]), the overall conversion efficiency at lower power levels could be increased. The proposed rectenna may become more efficient under realistic ambient environments. However, the output power in this case could still be very low, typically around 5 – 10 μ W, as reported in the previous papers [18], [19], [22], and [36]. Using such a low level power, many commercially available sensors could not work well. But in the future, some novel Nano-power sensors, circuits and devices might be available to use [33].

Apart from the wireless environmental sensors used in this work, other low power sensors such as PIR motion sensors, gas sensors, liquid sensors, smoke sensors and air pollution sensors [34] could also be powered by using the proposed clock rectenna harvester. Therefore, the clock products can be further developed for other applications. This will improve the functionality of such clocks. But, please be aware that the proposed clock rectenna is not necessarily the best option to power all the smart home sensors. Other compact and multiband rectennas could be used elsewhere [37].

V. PERFORMANCE COMPARISON

The performance comparison between the proposed energy harvesting clock rectenna and some latest multiband and broadband rectenna designs is given in Table II. Some related rectenna design examples for clocks and low power devices are also selected for comparison. It can be seen that our clock rectenna is the only design that utilizes the clock itself as the power receiving antenna, which eliminates the need of extra receiving antennas and arrays. Moreover, the proposed clock rectenna is one of the very few designs that have achieved relatively good performance without the aid of impedance matching networks. The presented method for the clock rectenna design is relative simple and innovative, while such a small modification on the conventional quartz clock products enables the potential of adding wireless energy harvesting function to charge the clock battery or to power wireless sensors. It should be noted that presented design is just a basic

example to show the new idea. The feed location and rectifier configuration can be further modified and optimized for other specific applications. For example, the feed location at $R2 = 10$ mm could be selected to cover the frequency bands at 1.6 and 2.1 GHz. Alternatively, the Schottky diodes used in this work could be substituted using other types of diodes for lower/higher input power levels (e.g., SMS7630 for input power < -15 dBm or HSMS2820 for input power > 15 dBm).

VI. CONCLUSION

A novel design method of adding the wireless energy harvesting feature to a quartz clock has been presented. Without introducing extra receiving antennas, the clock itself has been utilized as the power receiving device. Moreover, a simple rectifier has been introduced to directly match with the clock to form a complete clock rectenna. The measured results from a fabricated example have shown that the proposed clock rectenna has achieved good conversion efficiency and impedance matching performance over a range of frequency bands, input power levels and load values. The clock can harvest enough energy from a WiFi router to power a wireless environmental sensor. The sensors on the clock have demonstrated periodic wireless data transmissions by using the harvested power from the clock rectenna. Considering the outstanding performance of the clock rectenna in terms of its simplicity and functionality, the proposed design is very suitable for smart home applications. Also, the proposed method has shown an innovative and effective idea of designing such smart home furniture.

REFERENCES

- [1] Google Smart home products: (https://store.google.com/product/google_home_specs), 2017.
- [2] A. L. Bleda, F. J. Fernández-Luque, A. Rosa, J. Zapata and R. Maestre, "Smart sensory furniture based on WSN for ambient assisted living," *IEEE Sensors Journal*, vol. 17, no. 17, pp. 5626-5636, Sept., 1 2017.
- [3] M. J. Sanjari, H. Karami and H. B. Gooi, "Analytical rule-based approach to online optimal control of smart residential energy system," *IEEE Transactions on Industrial Informatics*, vol. 13, no. 4, pp. 1586-1597, Aug. 2017.
- [4] J. Pan, R. Jain and S. Paul, "A survey of energy efficiency in buildings and microgrids using networking technologies," *IEEE Communications Surveys & Tutorials*, vol. 16, no. 3, pp. 1709-1731, Third Quarter 2014.
- [5] S. D. T. Kelly, N. K. Suryadevara and S. C. Mukhopadhyay, "Towards the implementation of IoT for environmental condition monitoring in homes," *IEEE Sensors Journal*, vol. 13, no. 10, pp. 3846-3853, Oct. 2013.
- [6] A. Zanello, N. Bui, A. Castellani, L. Vangelista and M. Zorzi, "Internet of things for smart cities," *IEEE Internet Things J.*, vol. 1, no. 1, pp. 22-32, Feb. 2014.
- [7] Y. K. Tan and S. K. Panda, "Energy harvesting from hybrid indoor ambient light and thermal energy sources for enhanced performance of wireless sensor nodes," *IEEE Trans. Ind. Electron.*, vol. 58, no. 9, pp. 4424-4435, Sept. 2011.
- [8] M. R. Elhebeary, M. A. A. Ibrahim, M. M. Aboudina and A. N. Mohieldin, "Dual-source self-start high-efficiency microscale smart energy harvesting system for IoT," *IEEE Trans. Ind. Electron.*, vol. 65, no. 1, pp. 342-351, Jan. 2018.
- [9] L. V. Allmen et al., "Aircraft strain WSN powered by heat storage harvesting," *IEEE Trans. Ind. Electron.*, vol. 64, no. 9, pp. 7284-7292, Sept. 2017.
- [10] S. Kim et al., "Ambient RF energy-harvesting technologies for self-sustainable standalone wireless sensor platforms," *Proceedings of the IEEE*, vol. 102, no. 11, pp. 1649-1666, Nov. 2014.
- [11] K. Niotaki, A. Collado, A. Georgiadis, S. Kim and M. M. Tentzeris, "Solar/electromagnetic energy harvesting and wireless power transmission," *Proceedings of the IEEE*, vol. 102, no. 11, pp. 1712-1722, Nov. 2014.
- [12] S. Hemour and K. Wu, "Radio-frequency rectifier for electromagnetic energy harvesting: development path and future outlook," *Proceedings of the IEEE*, vol. 102, no. 11, pp. 1667-1691, Nov. 2014.
- [13] M. Zeng, A. S. Andrenko, X. Liu, Z. Li and H. Z. Tan, "A compact fractal loop rectenna for RF energy harvesting," *IEEE Antennas and Wireless Propagation Letters*, vol. 16, pp. 2424-2427, 2017.
- [14] H. Sun and W. Geyi, "A new rectenna using beamwidth-enhanced antenna array for RF power harvesting applications," *IEEE Antennas and Wireless Propagation Letters*, vol. 16, pp. 1451-1454, 2017.
- [15] T. Mitani, S. Kawashima and T. Nishimura, "Analysis of voltage doubler behavior of 2.45-GHz voltage doubler-type rectenna," *IEEE Transactions on Microwave Theory and Techniques*, vol. 65, no. 4, pp. 1051-1057, April 2017.
- [16] E. H. Shah, B. Brown and B. A. Cola, "A study of electrical resistance in carbon nanotube-insulator-metal diode arrays for optical rectenna," *IEEE Transactions on Nanotechnology*, vol. 16, no. 2, pp. 230-238, March 2017.
- [17] A. Y. S. Jou, R. Azadegan and S. Mohammadi, "High-resistivity CMOS SOI rectenna for implantable applications," *IEEE Microwave and Wireless Components Letters*, vol. 27, no. 9, pp. 854-856, Sept. 2017.
- [18] V. Palazzi et al., "A novel ultra-lightweight multiband rectenna on paper for RF energy harvesting in the next generation LTE bands," *IEEE Transactions on Microwave Theory and Techniques*, in press, 2017.
- [19] C. Song et al., "A novel six-band dual CP rectenna using improved impedance matching technique for ambient RF energy harvesting," *IEEE Transactions on Antennas and Propagation*, vol. 64, no. 7, pp. 3160-3171, July 2016.
- [20] P. Lu, X. S. Yang, J. L. Li and B. Z. Wang, "A compact frequency reconfigurable rectenna for 5.2- and 5.8-GHz wireless power transmission," *IEEE Trans. Power Electron.*, vol. 30, no. 11, pp. 6006-6010, Nov. 2015.
- [21] C. Song, Y. Huang, J. Zhou and P. Carter, "Improved ultrawideband rectennas using hybrid resistance compression technique," *IEEE Transactions on Antennas and Propagation*, vol. 65, no. 4, pp. 2057-2062, April 2017.
- [22] C. Song, Y. Huang, J. Zhou, J. Zhang, S. Yuan and P. Carter, "A high-efficiency broadband rectenna for ambient wireless energy harvesting," *IEEE Trans. Antennas Propag.*, vol. 63, no. 8, pp. 3486-3495, Aug. 2015.
- [23] J. J. Trad, B. A. Zeb, K. P. Esselle and M. U. Afzal, "Preliminary investigations into a simple and effective rectenna for RF energy harvesting," *2017 IEEE International Symposium on Antennas and Propag. & USNC/URSI National Radio Science Meeting*, San Diego, CA, 2017, pp. 1095-1096.
- [24] J. A. C. Theeuwes, H. J. Visser, M. C. van Beurden and G. J. N. Doodeman, "Efficient, compact, wireless battery design," *2007 European Conference on Wireless Technologies*, Munich, 2007, pp. 233-236.
- [25] S. V. Cataldo and N. C. Karmakar, "Wireless battery design for clock and DC motor," *Asia-Pacific Microwave Conference, Macau*, 2008, pp. 1-4.
- [26] <https://www.woodcraft.com/categories/clock-supplies>
- [27] W. A. Marrison and J. W. Horton, "Precision determination of frequency," *I.R.E. Proc.* vol. 16, no. 2, pp. 137-154, Feb. 1928.
- [28] C. Song et al., "Matching network elimination in broadband rectennas for high-efficiency wireless power transfer and energy harvesting," *IEEE Trans. Ind. Electron.*, vol. 64, no. 5, pp. 3950-3961, May 2017.
- [29] J. O. McSpadden, Lu Fan and Kai Chang, "Design and experiments of a high-conversion-efficiency 5.8-GHz rectenna," *IEEE Trans. Microw. Theory Techn.*, vol. 46, no. 12, pp. 2053-2060, Dec 1998.
- [30] *BQ25504 Ultra Low Power Boost Converter with Battery Management for Energy Harvester*, Technical datasheet, Texas Instrument, Jun. 2015.
- [31] *Scavenger transmitter module, STM 330 / STM 331 / STM 332U / STM 333U*, User manual, Enocean, Aug. 2015.
- [32] *DolphinView overview*, User manual, Enocean, Aug. 2015.
- [33] M. Dini, A. Romani, M. Filippi and M. Tartagni, "A Nanocurrent Power Management IC for Low-Voltage Energy Harvesting Sources," *IEEE Trans. Power Electron.*, vol. 31, no. 6, pp. 4292-4304, Jun. 2016.
- [34] http://www.libelium.com/libeliumworld/smart_cities/ Libelium smart city development kits, Jan. 2018.
- [35] <http://energous.com/technology/transmitters/> WattUP transmitters, 2018.
- [36] C. H. P. Lorenz et al., "Breaking the efficiency barrier for ambient microwave power harvesting with heterojunction backward tunnel

diodes," *IEEE Trans. Microw. Theory Techn.*, vol. 63, no. 12, pp. 4544–4555, Dec. 2015.

- [37] C. Song, Y. Huang, P. Carter, J. Zhou, S. Joseph and G. Li, "Novel Compact and Broadband Frequency-Selectable Rectennas for A Wide Input-Power and Load Impedance Range," *IEEE Trans. Antennas Propag.*, in press, 2018.



Chaoyun Song (S'16–M'17) received the M.Sc. degree and PhD degree in electrical engineering and electronics from The University of Liverpool (UoL), Liverpool, U.K., in 2013 and 2017.

He was as a Research Assistant and Antenna Design Engineer at the UoL and BAE systems, Chelmsford, UK during 2015-2016. He is currently a Postdoctoral Research Associate at the UoL, UK. He has authored/co-authored more than 30

papers in internationally refereed journals and conference proceedings. He has filed 6 US, EU and UK patents. He received many international awards such as the winner of the IET Present Around the World Competition (2016) and the EW Bright-Sparks Award for outstanding electronic engineers under age 30 in the UK (2018). He won the BAE Systems Chairman's Award in 2017 for the innovation of next generation GNSS antennas. His current research interests include liquid antennas, novel materials, wireless energy harvesting, rectifying antennas, wireless power transfer, GNSS antennas and anti-jamming technologies and smart sensors for the IoT.

Dr. Song has been a regular reviewer of more than 10 international journals including Applied Physics Letters, Scientific Reports, IEEE Transactions on Antennas and Propagation, IEEE Transactions on Industrial Electronics, IEEE Transactions on Microwave Theory and Techniques, IEEE Transaction on Circuits and Systems I: Regular Papers, IEEE Antennas and Wireless Propagation Letters and IEEE Sensors letters.



Ana López-Yela was born in Madrid (Spain) on July 12, in 1991. She received the B.S. degree in Electrical Engineering from the Technical University of Madrid (UPM) in 2013, and the dual M.S degrees in Telecommunications Engineering and in Multimedia and Communications in 2015 from University Carlos III of Madrid (UC3M). She is currently pursuing the Ph.D. degree in the Group

of Radiofrequency, Electromagnetism, Microwaves and Antennas (GREMA) at UC3M. Her work is focused on electrically small antennas for aircraft communications and also in broadband rectennas for energy harvesting applications.



Yi Huang (S'91–M'96–SM'06) received the D.Phil. degree in communications from the University of Oxford, Oxford, U.K., in 1994.

He has been conducting research in the areas of wireless communications, applied electromagnetics, radar, and antennas since 1987. He was with NRIET, as a Radar Engineer and spent various periods with the Universities of Birmingham, Oxford, and Essex, U.K. as a Member of Research Staff. In

1994, he joined British Telecom Labs, as a Research Fellow. In 1995, he joined the Department of Electrical Engineering and Electronics, University of Liverpool, Liverpool, U.K., as a faculty member, where he is currently a Full Professor in Wireless Engineering, the Head of the High Frequency Engineering Group and Deputy Head of Department. He has authored over 300 refereed papers in leading international journals and conference proceedings, and authored *Antennas: From Theory to Practice* (Wiley, 2008) and *Reverberation Chambers: Theory and Applications to EMC and Antenna Measurements* (Wiley, 2016).

Prof. Huang is a Senior Fellow of the HEA. He is a Fellow of the IET. He has received many research grants from research councils, government agencies, charity, EU and industry, acted as a consultant to various companies, and served on a number of the national and international technical committees and has been an Editor, Associate Editor, or Guest Editor of four international journals. He has been a

keynote/invited speaker and organizer of many conferences and workshops (e.g., WiCom 2006, 2010, IEEE iWAT2010, and LAPC2012). He is currently the Editor-in-Chief of *Wireless Engineering and Technology*, Associate Editor of *IEEE Antennas and Wireless Propagation Letters*, U.K., and Ireland Rep to the European Association of Antenna and Propagation (EurAAP).



Daniel Segovia-Vargas (M'98) was born in Madrid, Spain, in 1968. He received the Telecommunication Engineering Degree and the Ph.D. degree from the Polytechnic University of Madrid, Madrid, in 1993 and in 1998, respectively.

From 1993 to 1998 he was assistant professor at the University of Valladolid. Since 1998 he is a professor at the Carlos III University, where he teaches Microwave and High Frequency Circuits and Antennas. From 2004 to 2010 he was Director of Telecommunications Engineering of the Polytechnic School of the UC3M and from 2012 Director of the Polytechnic School of the Carlos III University of Madrid.

Prof. D. S.-Vargas has authored more than 150 journal publications and international conference. His research interests include antennas, active antennas, THz metamaterials and technologies. He has been the president and organizer of URSI2011, a member of the Organizing Committee EuCAP 2010, and has organized several international workshops in the field of THz metamaterials and technologies. He is a national delegate of the Cost actions in the field of antennas (Cost 284 Cost IC0603, IC1102 Cost) since 2002.



Yuan Zhuang was born in Baoding, Hebei, China, in 1991. He received the B.Eng degree (Hons) in telecommunication engineering from Xi'an Jiao Tong Liverpool University, Suzhou, China, and University of Liverpool, Liverpool, United Kingdom in 2014. He is currently working toward the Ph.D. degree in the department of electrical engineering and electronics at the University of Liverpool, Liverpool, UK.

His research interests include microwave power amplifiers, filters, electromagnetic energy harvesting and wireless energy transfer.



Yansong Wang received the B.Eng. (Hons.) degree in electrical and electronic engineering from Xi'an Jiao Tong Liverpool University, Suzhou, China, and University of Liverpool, Liverpool, United Kingdom in 2017. He is currently working towards a Ph.D. degree in the Department of Electrical Engineering and Electronics at the University of Liverpool, Liverpool, UK.

His research interests include novel sensor designs, low power wide area networks and wireless sensor networks



Jiafeng Zhou received the Ph.D. degree from the University of Birmingham, Birmingham, U.K., in 2004.

He was with the National Meteorological Satellite Centre of China, Beijing, China, from 1997, for two and a half years, where he was involved in the development of communication systems for Chinese geostationary meteorological satellites. From 2004 to 2006, he was a Research Fellow with the University of Birmingham, where he was involved in phased arrays for reflector observing systems. He then moved to the Department of Electronic and Electrical Engineering, University of Bristol, Bristol, U.K., until 2013, where he was involved in the development of highly efficient and linear amplifiers. He is currently with the Department of Electrical Engineering and Electronics, The University of Liverpool, Liverpool, U.K. His current research interests include microwave power amplifiers, filters, electromagnetic energy harvesting, and wireless power transfer.